High Harmonic Generation near the Low-Frequency Edge of a Plateau under Nonlinear Propagation of 1.24-µm Near-Infrared Femtosecond Laser Radiation in a Dense Argon Jet

B. V. Rumiantsev[a, *], A. V. Pushkin[a], and F. V. Potemkin[a]

[a] Faculty of Physics, Moscow State University, Moscow, 119991 Russia
*e-mail: rumjancev.bv15@physics.msu.ru

High (15−25) harmonic generation in the vacuum ultraviolet spectral range (83−50 nm) has been realized by focused (NA = 0.033) near-infrared femtosecond laser radiation (wavelength λ = 1.24 µm) with a vacuum intensity of ~7.5×10^{14} W/cm^2 irradiating a dense gas jet. It has been shown experimentally that the use of such a high-numerical aperture focusing requires high (up to 10 bar) gas jet pressures to optimize phase matching. The use of the dense gas jet results in a noticeable manifestation of nonlinear propagation effects for generating radiation, which affect the generation process through the change in the phase matching conditions. Furthermore, it has been shown that the prechirping of the generating pulse makes it possible to compensate a chirp appearing due to self-phase modulation and to increase the harmonic generation efficiency because of the nonlinear compression of the generating pulse. This approach has allowed 17th (73 nm) harmonic generation with an energy of 2 pJ in a pulse and a generation efficiency of 5.4×10^{-9}. The estimates obtained have shown that this radiation can be used for single-pulse maskless photolithography in the extreme ultraviolet range.

INTRODUCTION

High harmonic generation in the field of intense ($10^{14}-10^{15}$ W/cm^2) femtosecond laser radiation is currently under active studies in laser physics and nonlinear optics. High harmonic generation is based on fundamental aspects of the interaction of laser radiation with matter in the plasma-formation regime, which lie at the junction of laser physics, nonlinear optics, quantum theory, and atomic physics; thus, this field of physics is of fundamental significance. high harmonic generation is also important for applications: sources based on this effect are currently the only table tools both to obtain coherent radiation in the vacuum ultraviolet [1] and soft X-ray [2] ranges and to generate attosecond (10^{-18} s) pulses [3].

The main method to control the temporal shape, polarization state, and efficiency of high harmonic generation is to vary the temporal shape of the generating pulse field by, e.g., a two-color laser excitation. In particular, the addition of the second harmonic to the main pulse breaks the symmetry of the acting laser field and leads to the generation of both even and odd harmonics [4]. Moreover, the use of two-color fields with different polarization states allows the generation of elliptically polarized harmonics [5]. The supplement of the main generating radiation with an intense terahertz pulse as a strong quasistatic field is of partic-

ular interest [6]. In particular, it was shown theoretically that this allows one to expand the spectrum of the generated harmonics [7] with the simultaneous generation of even harmonics due to the terahertz-field-induced breaking of the symmetry of the interaction [8], which was also demonstrated experimentally [9].

The most widespread sources of generating radiation are currently laser systems based on the Ti:sapphire crystal (wavelength of about 0.8 µm) and on Yb-doped crystals (wavelength of about 1 µm) [10]. These systems are commercially available and can operate at a high (up to megahertzs [11]) repetition rate, which makes it possible to increase the average power of the generated harmonics in order to compensate their low peak power. To achieve a longer-wavelength range, which is necessary for the expansion of the harmonic spectrum [12], nonlinear optical schemes based on the parametric conversion of the radiation frequency of a near infrared source [13]. Such schemes feature the necessity of a fine alignment for the selection of the appropriate wavelength, as well as an additional decrease in the resulting harmonic generation efficiency due to an additional cascade of the nonlinear optical conversion of the wavelength of generating radiation.

An alternative approach to increase the wavelength of generating radiation is the application of laser sys-

tems directly generating long-wavelength near- and mid-infrared radiation, in particular, laser systems based on the Cr:forsterite (wavelength of 1.24 μm) and Fe:ZnSe (wavelength of 4.5 μm) [14] crystals, which were already used to generate low harmonics [15–18] and are promising sources of shorter-wavelength radiation through high harmonic generation. In this context, in this work, high harmonic generation is induced for the first time by radiation of a laser system based on the Cr:forsterite crystal.

High harmonic generation induced by long-wavelength radiation requires the careful optimization of the generation process because the response of a single atom to the applied laser field in the process of high harmonic generation decreases with increasing wavelength as λ^{-x}, where $x = 5$–6 [12]. This effect can be compensated by, e.g., increasing the density of the gas medium, which makes it possible to increase the number of atoms of the medium involved in the interaction. The increase in the density of the gas medium enhances the nonlinear propagation effects of generating radiation. Consequently, the experimental implementation of high harmonic generation with long-wavelength radiation requires the study of the influence of nonlinear propagation effects on the generation process.

The influence of nonlinear effects on the process of high harmonic generation was studied both theoretically and experimentally. In particular, the authors of [19] presented the 3D + 1 numerical model of high harmonic generation taking into account the propagation of generating radiation and harmonics under the effect of Kerr nonlinearity and plasma generation. This model, where the microscopic response is calculated in the quantitative rescattering approach, correctly describes the experimental harmonic spectra and allows one to reconstruct the spectrum corresponding to the microscopic response of an atomic or molecular medium. A similar model was proposed in [20], where the microscopic response is calculated in an approach based on the density functional theory. The authors of [21] demonstrated theoretically and experimentally that harmonic generation in the self-channeling regime and with the corresponding restriction of the intensity of generating laser radiation at a wavelength of 1.8 μm leads to the limitation of the cutoff frequency but makes it possible to increase the generation efficiency due to an increase in the length of the effective interaction region and to form a collimated harmonic radiation beam in the energy range of 50–550 eV. The authors of [22] detected a change in the spectrum of generating near infrared radiation in a relatively long (30 cm) path under harmonic generation.

Unlike the cited works, we focus here on the experimental study both of the influence of nonlinear propagation effects on phase matching in the process of high harmonic generation in the dense gas jet and of the possibility of using these effects to increase the generation efficiency.

EXPERIMENTAL SETUP

The layout of the experimental setup is presented in Fig. 1. We used radiation from a femtosecond laser system based on the Cr:forsterite crystal (wavelength 1.24 μm, FWHM pulse duration 110 fs, pulse energy up to 3.5 mJ, pulse repetition rate 10 Hz). To vary the generating radiation energy, we used a half-wave plate together with a polarizer, which were placed in front of the compressor of the laser system. Radiation passing through a thin SiO_2 window entered the detection chamber, where it was focused by a lens with a focal length of 100 mm in a focusing regime with a numerical aperture of NA = 0.033 on the pulsed argon jet in the generation chamber. Such a focusing with a relatively high numerical aperture ensured the approximate coincidence of the length of the generation medium ($L \approx 500$ μm) with the confocal parameter ($2z_R \approx 700$ μm, where z_R is the Rayleigh length) of generating radiation, which made it possible to optimize the generation efficiency [16], but, at the same time, ensured a nonzero contribution from the geometric phase within the phase matching. The vacuum intensity at the waist reached $\sim 7.5 \times 10^{14}$ W/cm² at the maximum utilized energy of the generating pulse of 400 μJ. An Al filter was placed behind the generation chamber to block generating radiation and to pass harmonic radiation in the photon energy range of ~15–70 eV. Transmitted harmonic radiation was incident on the
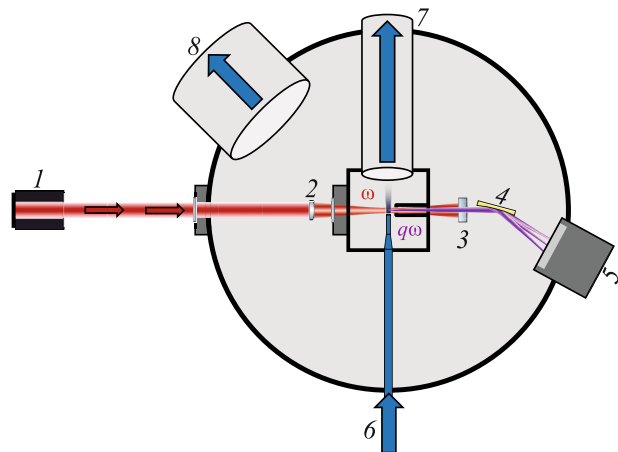

Fig. 1. (Color online) Layout of the experimental setup: (*1*) laser system based on the Cr:forsterite crystal (central wavelength 1.24 μm, FWHM pulse duration is 110 fs, pulse energy is up to 3.5 mJ, pulse repetition frequency 10 Hz); (*2*) lens with a focal length of 100 mm; (*3*) Al filter; (*4*) 300-grooves/mm concave diffraction grating; (*5*) camera to detect harmonics; (*6*) argon supply; (*7*) pumping of the supplied gas from the generation chamber; and (*8*) pumping of the supplied gas from the detection chamber.
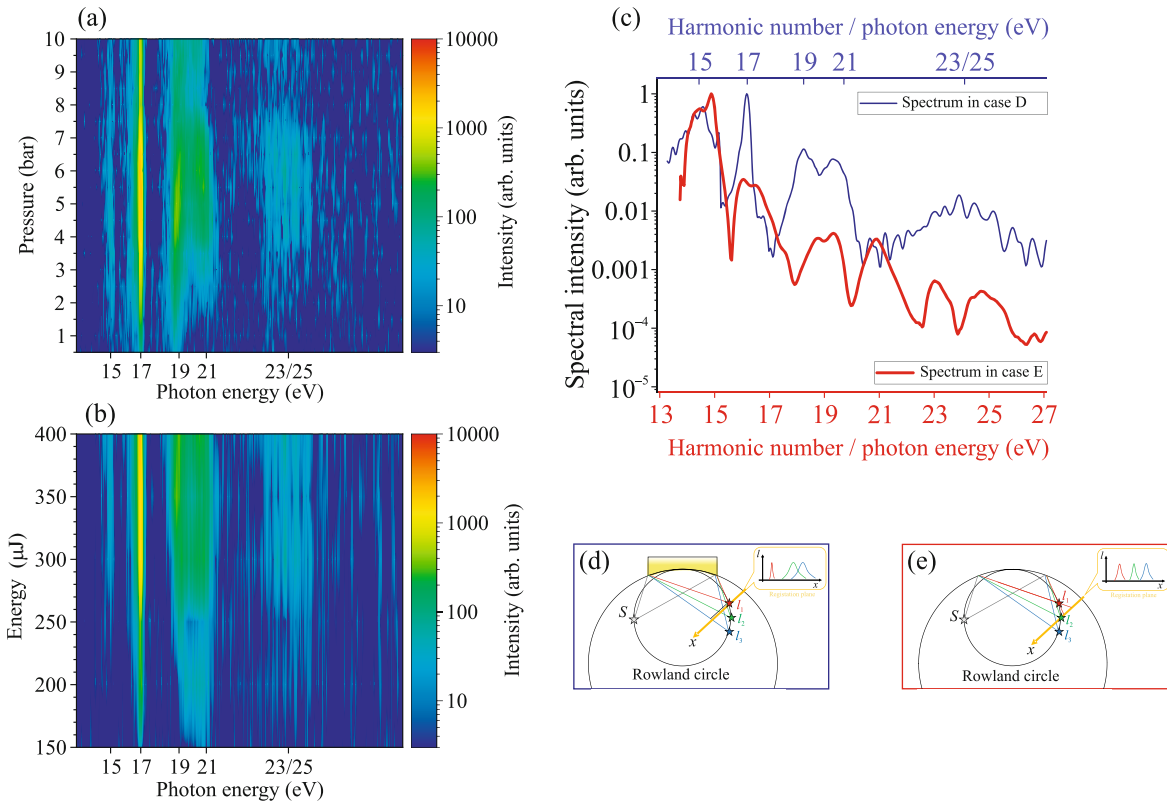
Fig. 2. (Color online) (a) Detected harmonic spectrum versus the argon pressure at a generating pulse energy of 400 μJ. (b) Detected harmonic spectrum versus the generating pulse energy at an argon pressure of 5.5 bar. (c) Detected harmonic spectrum at a generating pulse energy of 400 μJ, an argon pressure of 5.5 bar, under two distances between the grating and the detection plane corresponding to the detection schemes (d, e). (d, e) Detection schemes for diffracted harmonic radiation with the concave diffraction grating together with the plane detecting matrix of the camera: (S) point source, which is the waist of generating radiation on the gas target and (l_1, l_2, l_3) foci of harmonics 1, 2, 3, respectively. The detection of radiation focused on the Rowland circle by the plane matrix at a distance between the grating and the detection plane when one of the side harmonics is at the focus (see panel (d)) results in the imposition of spectral components whose foci are located not on the detection plane. An increase in the distance between the grating and the detection plane makes it possible to avoid the imposition of spectral components due to the shift of the focus towards higher photon energies (panel (e)).

concave diffraction grating. Diffracted harmonic radiation was detected by a Dhyana XF95 camera. The resolution of this system taking into account the linear dispersion at the focus of the grating and the camera pixel size is higher than $\lambda/\delta\lambda = 2000$. The wavelength of generated harmonic radiation was calibrated using the transmission spectrum of the Al filter, and the energy of detected radiation was calibrated using the quantum efficiency of the camera and the transmission spectrum of the filter.

RESULTS AND DISCUSSION

Using the described experimental setup, we generated and detected the 15th (83 nm), 17th (73 nm), 19th (65 nm), 21st (59 nm), 23rd (54 nm), and 25th (50 nm) harmonics (Fig. 2c). The dependences of the harmonic spectrum on the gas jet pressure and generating pulse energy are shown in Figs. 2a and 2b, respectively.

As seen in Figs. 2a and 2b, the spectrum of the generated radiation strongly depends on the gas jet pressure and the generating pulse energy. The maximum energy yield of harmonics was reached at a pressure of 5.5 bar and a pulse energy of 400 μJ. The spectrum of the detected radiation at these parameters is presented in Fig. 2c. The harmonic numbers coincide with the corresponding photon energies in electronvolts because the wavelength of generating radiation (1.24 μm) corresponds to a photon energy of 1 eV.

The blue line in Fig. 2c presents the spectrum detected at the distance between the grating and the detection plane such that the 17th harmonic, which is one of the side harmonics, is at the focus. In this case, the 15th, 17th, 19th, and 21st harmonics are resolved in the detected spectrum. With an increase in the harmonic number, the spectral components are merged due to the decrease in the resolution of the detection system and, as seen for the 23rd and 25th harmonics, can completely overlap with each other, giving an

interference pattern in the spectrum. The decrease in the resolution of the detection system with increasing harmonic number is explained by the features of the detection system because the diffracted harmonic radiation focused on the Rowland circle (see the inset of Fig. 2d) is detected by a plane matrix and the effective linear dispersion of the grating decreases beyond the focal plane.

An increase in the distance between the grating and the detection plane (Fig. 2e) leads to the displacement of the focus towards higher harmonics, which, according to the red line in Fig. 2c, makes it possible to increase the spectral resolution for the 23rd and 25th harmonics, but the resolution of the 15th and 17th harmonics decreases. In addition, we took into account the difference of the shape of the detection plane from the focusing surface of the grating the coordinate along which is approximately described as $y(x) = y_0 + ax^2$, where x is the coordinate along the detection plane; this allowed the linearization of the photon energy scale and to obtain the equidistant distribution of harmonics.

The absence of higher harmonics in the spectrum (up to ~350 eV at a reached vacuum intensity of ~7.5×10^{14} W/cm^2) can be explained by two factors. The first factor is that higher harmonics reach the matrix under the conditions of the divergent wavefront behind the focus; as a result, the intensity of these harmonics is beyond the dynamic detection range. The second factor is the use of a comparatively long pulse (110 fs, 27 field cycles) for generation, which can violate phase matching conditions for higher harmonics due to the formation of the plasma by the leading edge of the pulse.

As seen in Fig. 2c, the 17th harmonic has the smallest spectral width among all detected harmonics. Therefore, its focus at the detection is closer to the detection plane than the others; for this reason, experimental dependences are presented below for this harmonic.

One of the main parameters affecting the macroscopic response of the medium in the process of harmonic generation is the density of the gas jet, which is determined by the gas pressure applied to the target. The dependence of the generation efficiency of the qth harmonic on the pressure is given by the expression [23]

$$I_q \propto |pF_q(p)|^2, \qquad (1)$$

where

$$F_q(p) = \int_{-L/2}^{L/2} \frac{e^{i(\Delta k(p)z' - (q-1)\arctan(z'/z_R))}}{\left(1 + (z'/z_R)^2\right)^{\frac{q-1}{2}}} dz' \qquad (2)$$

is the phase matching integral, L is the length of the medium, z_R is the Rayleigh (diffraction) length, and $\Delta k(p) = qk_1(p) - k_q(p)$ is the scalar mismatch between the wave vectors of the qth harmonic and the qth order polarization. According to Eq. (2), the maximum energy of the qth harmonics is reached when the exponent in Eq. (2) is zero, i.e., under the condition

$$\Delta k(p)z' - (q-1)\arctan(z'/z_R) = 0, \qquad (3)$$

which is the phase matching condition of harmonic generation by the focused Gaussian beam. In Eq. (3), the first term is responsible for the phase mismatch between the qth harmonic and the qth order polarization wave, which is due to the material dispersion of the medium and the dispersion of the plasma induced by the generating pulse, and the second term is the geometric phase. It is noteworthy that the satisfaction of this condition for all points $z \in [-L/2; L/2]$ simultaneously is possible only under $L \ll 2z_R$. Otherwise, the condition (3) cannot be satisfied for all points of the medium simultaneously; hence, it is reasonable to consider the satisfaction of this condition on average over the length of the medium L.

We emphasize that Eqs. (1)−(3) describe only phase matching for the process of harmonic generation and do not describe the response of a single atom to a strong light field and nonlinear propagation effects. A more accurate simulation including the description of these effects was performed in [24]. Taking into account the response of a single atom, which was determined in the three-dimensional simulation of the time-dependent Schrödinger equation, change in the pulse shape in the partially ionized gas medium, and the effect of the gas pressure and the type of the atom, the authors of [24] carried out self-consistent numerical calculations of the propagation of a pulse with a central wavelength of 810 nm in the near infrared range and a duration of 15−40 fs in argon and neon.

Since the refractive index and the atomic density in the medium in the pressure range, where the medium holds its aggregate state, are linear functions of the pressure, the mismatch between the wave vectors can be written in the form

$$\Delta k(p) = p\Delta k_{1bar} = p\left(\Delta k_{1bar}^{mat} - \Delta k_{1bar}^{plasma}\right), \qquad (4)$$

where Δk_{1bar} is the pressure-normalized mismatch between the wave vectors at a pressure of 1 bar and Δk_{1bar}^{mat} Δk_{1bar}^{plasma} are the corresponding contributions to this mismatch from the material dispersion and induced plasma, respectively. Efficient harmonic generation occurs under the condition (3), which is possible only if $\Delta k_{1bar} = \Delta k_{1bar}^{mat} - \Delta k_{1bar}^{plasma} > 0$. This inequality can be satisfied only when the frequencies of generating radiation and its harmonics are on the different sides from the electron resonance of the generation medium, which is characteristic of high-order harmonics rather than of low harmonics. According to

Eq. (3), the integral in Eq. (2) and, as a result, the intensity of the qth harmonic are maximal at the optimal pressure

$$p_{max} = \frac{(q-1)\arctan(z'/z_R)}{\Delta k_{1bar} z'}. \tag{5}$$

An increase in the ionization degree of the medium with the intensity of the generating pulse will reduce the difference between Δk_{1bar}^{mat} and Δk_{1bar}^{plasma} decrease the parameter Δk_{1bar} and correspondingly increase the optimal pressure p_{max} [24]. We emphasize that the situation in the case of low harmonic generation is opposite [18] because the frequencies of harmonics and the main radiation are on the same side from the electron resonance of the medium.

In the low-pressure region, where the effect of the phase matching integral (2) is small, the energy of harmonics increases with the pressure as $I_q \propto p^2$ (see (1)). A further increase in the pressure enhances the effect of the phase matching integral due to the increase in the contribution of the material dispersion of the medium and the dispersion of the laser-induced plasma $\Delta k(p)$, which results in the deviation from the law $I_q \propto p^2$. The subsequent increase in the pressure leads to the compensation of the geometric phase, to the corresponding achievement of the phase matching condition (3), and to the maximum energy yield of harmonics at the optimal pressure (5). The further increase in the pressure violates the phase matching condition (3), which reduces the harmonic generation efficiency. In this case, the dependence $I_q(p)$ demonstrates oscillations with a period corresponding to the phase $2\pi/L$ of the complex exponential in Eq. (2). The described behavior was observed in our experiment for high harmonics at relatively low (150–250 μJ) generating pulse energies (Fig. 3). As seen in Fig. 3, the increase in the generating pulse energy above 300 μJ results in the deviation from the law $I_q \sim p^2$ at low pressures, which is observed at lower energies. A similar effect was also observed for low harmonics [15]; consequently, the mentioned deviation can also be explained by increasing role of nonlinear propagation effects with increasing generating pulse energy. Furthermore, as seen in Fig. 3, the optimal pressure p_{max} increases with the generating pulse energy according to Eq. (5) only in the energy range up to 300 μJ. The subsequent increase in the energy does not lead to the increase in the optimal pressure, which remains 5.5–6 bar because the reached intensity is limited by nonlinear propagation effects such as self-phase modulation, self-focusing, and plasma generation. All these effects can lead to the quasifilament propagation regime of the generating pulse near the target, as well as to the corresponding restriction of the intensity [25] and to the decrease in the geometric phase in Eq. (3).
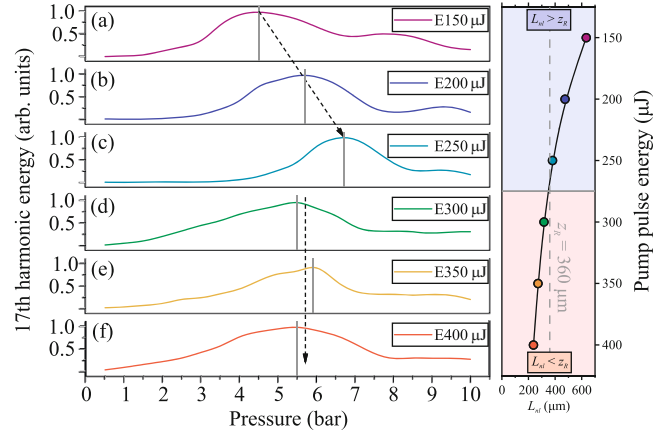
Fig. 3. (Color online) Experimental energy of the 17th harmonic versus the argon jet pressure for generating pulse energies of (a–f) 150–400 μJ. The right inset shows the nonlinear length calculated from the experimental data versus the generating pulse energy. It is seen that the optimal pressure ceases to increase and is fixed at 5.5–6 bar when the nonlinear length decreases below the diffraction length z_R.

Indirect evidence of this propagation regime is that, as the energy increases from 250 to 300 μJ, the nonlinear length L_{nl} decreases from 380 to 320 μm and becomes shorter than the diffraction length $z_R = 360$ μm (Fig. 3).

In addition, oscillations in the experimental dependence $I_q(p)$ in a given pressure region disappear at higher energies of laser radiation (300–400 μJ). This behavior can be attributed to a significant increase in the period of oscillations at high (above 5.5–6 bar) pressures, which can be due to a decrease in the difference between the contributions from the material, Δk_{1bar}^{mat}, and plasma, Δk_{1bar}^{plasma}, dispersions in Eq. (4) because of the increase in the degree of ionization with the efficiency of avalanche ionization.

The approximation of the pressure dependence of the energy of the 17th harmonic (Fig. 3) according to Eqs. (1)–(4) allowed us to determine the average degree of ionization over the generation region length and the corresponding electron density in the generated plasma (Fig. 4). The plot in Fig. 4 indicates that the degree of ionization of the medium increases with the generating pulse energy and the degree of ionization is saturated at high energies of 300–400 μJ. This behavior can be explained by intensity clamping upon quasifilament radiation propagation near the target. The calculation of the balance of effective additions to the refractive index also confirms this possibility. In particular, the authors of [26] showed that balance between Kerr self-focusing, plasma defocusing, and
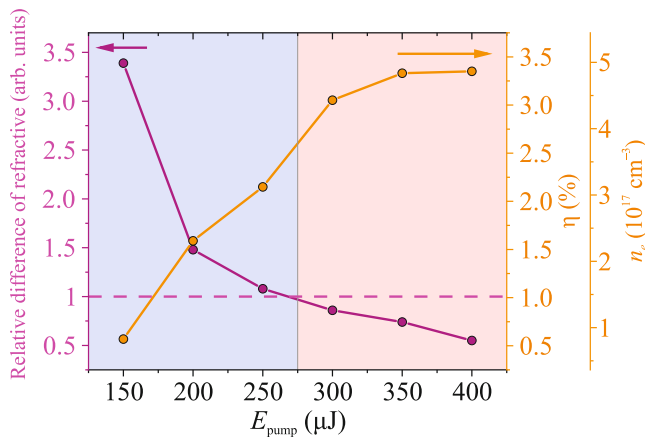
Fig. 4. (Color online) (Violet line) Relative difference of effective correction to the refractive index due to the Kerr self-focusing, plasma defocusing, and diffraction at a pressure of 6 bar calculated from the experimental data versus the generating pulse energy. (Orange line) Ionization degree of the medium and the electron density in the plasma at a pressure of 6 bar calculated from the experimental data versus the generating pulse energy.

diffraction, which is necessary for the filamentation propagation regime, is reached under the condition

$$\Delta(\delta n) = n_2 I - \frac{n_e}{2n_{cr}} - \frac{(1.22\lambda)^2}{8n\pi w_0^2} = 0. \quad (6)$$

Here, the first, second, and third terms are the effective additions to the refractive index due to Kerr self-focusing, plasma defocusing, and diffraction, respectively; n_2 is the nonlinear refractive index, I is the radiation intensity, n_e is the electron density in the plasma, n_{cr} is the critical electron density of the plasma, λ is the wavelength of radiation, n is the linear refractive index, and w_0 is the radius of the beam waist. Since the condition (6) cannot be exactly satisfied in experiments, the balance condition (6) for experimental data can be quantitatively characterized by the relative difference between corrections, which is defined as

$$\Delta(\delta n)_{rel} = \frac{\Delta(\delta n)}{\min(\delta n_{kerr}, \delta n_{plasma}, \delta n_{dif})}, \quad (7)$$

where $\min(\cdot)$ is the minimum of the parameters in the parentheses. If this relative difference is smaller than unity, the balance condition (6) can be considered as fulfilled. Using the experimental electron density of the plasma, we plotted the dependence of the relative difference between the corrections to the refractive index on the generating pulse energy (see Fig. 4). This dependence shows that the increase in the energy from 250 to 300 μJ leads to the decrease in the difference between the corrections below unity, indicating the satisfaction of the contribution balance condition (6) and the possibility of the quasi-filament propagation regime. It is noteworthy that the saturation of the

degree of ionization in the medium also begins near an energy of 300 μJ (Fig. 4), which can additionally indicate intensity saturation in this propagation regime. Thus, the electron densities in the plasma, which are determined from the experimental pressure dependences of the energy of the 17th harmonic (see Fig. 3), in combination with the experimental parameters of radiation, medium, and focusing confirm the possibility of the quasifilament propagation regime of generating radiation, which can explain the deviation of experimental dependences from theoretical ones at high energies of 300−400 μJ.

A significant influence of nonlinear propagation effects on the process of harmonic generation in this work is due to the use of a dense gas jet as a target. A high pressure up to 10 bar applied to the jet is necessary for the compensation of the contribution from the geometric phase to the phase matching condition (3) in the case of focusing with a relatively high (NA = 0.033) numerical aperture [27]. Another manifestation of nonlinear propagation effects is the detected spectral broadening of harmonics with increasing pressure (Fig. 5), which was also observed previously in experiments on low harmonic generation [15]. As seen in Fig. 5, an increase in the pressure leads to the linear increase in the spectral width of the 17th harmonic, which can be attributed to phase modulation due to the Kerr effect [23]. The spectral broadening of the harmonics in the general case can be due to the self-phase modulation of generating radiation, to the direct self-phase modulation of harmonic radiation, and to the cross-modulation of harmonic radiation by the generating pulse. However, since the self-phase modulation effect strongly depends on the wavelength and intensity of radiation [28], the most probable mechanism of the observed broadening of the harmonics is the self-phase modulation of generating radiation.

The self-phase modulation leads not only to the spectral broadening of the harmonics, but also to the formation of a positive chirp in their phase spectra and in the phase spectrum of the generating pulse [28]. The negative chirp of the generating pulse can compensate a positive chirp appearing due to the self-phase modulation, which makes it possible to increase the peak intensity of the generating pulse due to the reduction of its duration in the process of self-phase modulation and, thus, to increase the generation efficiency. This effect was observed in our study (Fig. 6). As seen in Fig. 6a, the maximum generation efficiency is reached with the introduction of the negative chirp in the generating pulse. In this case, according to the plot in Fig. 6b and Table 1, the presented dependence of the energy of the harmonics on the chirp is asymmetric with respect to an optimal value of −124 fs. In particular, a slow hyperbolic dependence is observed in the region of the positive chirp. A faster hyperbolic dependence is observed in the region of the negative chirp, which indicates a faster change in the duration
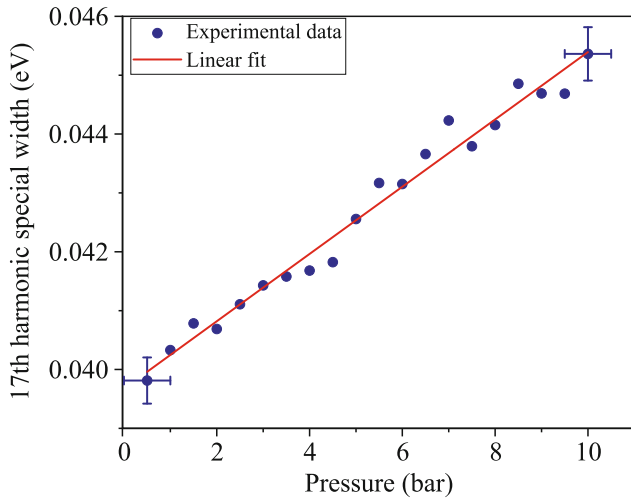
Fig. 5. (Color online) Spectral width of the 17th harmonic versus the argon jet pressure at a generating pulse energy of 400 μJ.
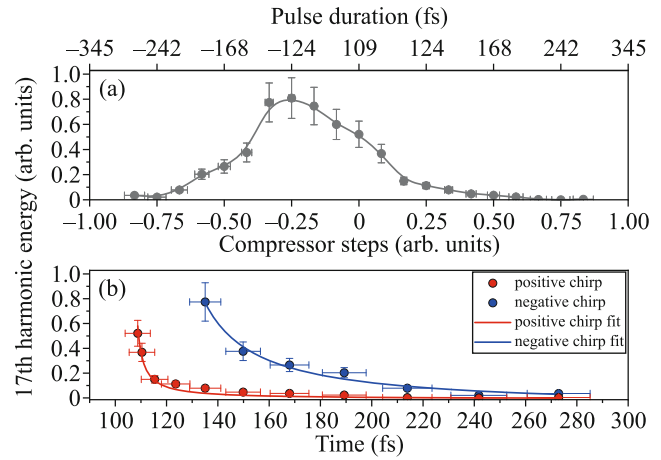

Fig. 6. (Color online) (a) Energy of the 17th harmonic versus the duration varying by chirping the generating laser pulse. Negative durations correspond to a negative chirp. (b) Approximation of the energy of the 17th harmonic versus the laser pulse duration at the (red line) positive and (red line) negative chirps. The approximation parameters are summarized in Table 1.

of the generating pulse under the variation of the chirp in this region due to an additional effect of the nonlinear compression caused by the self-phase modulation.

The maximum achieved energy and the corresponding generation efficiency are 3.6 pJ and 9.7×10^{-9} for the 15th harmonic and 2 pJ and 5.4×10^{-9} for the 17th harmonic, respectively. The energy of the harmonics was calculated by the formula

$$E = \sum_{i,j} \frac{I(x_i, y_j) - I_0}{QE(\lambda)C} \frac{\Delta t_{int}}{\Delta t_{rep.rate}}, \qquad (8)$$

where $I(x_i, y_j)$ is the intensity of the pixel with the coordinates (x_i, y_j), I_0 is the dark noise of the camera averaged over pixels, $QE(\lambda)$ is the quantum efficiency of the matrix at the wavelength λ, C is the coefficient for the recalculation of the pixel intensity to the number of photoelectrons, Δt_{int} is the exposure time, $\Delta t_{rep.rate}$ is the repetition period of laser pulses, and summation is performed over all pixels of the matrix near the signal of the harmonics. The focusing of radiation of the 17th harmonic with an energy of 2 pJ into a spot with a diffraction-limited radius (73 nm) using an optical device with NA = 0.33, which is already available in the extreme ultraviolet range [29], will

allow the achievement of an energy density of 24 mJ/cm² in a pulse. This energy density is comparable with a dose of 10−30 mJ/cm² used for irradiation of a photoresist in modern extreme ultraviolet photolithography systems, where spatially incoherent radiation, which is generated due to the ablation of the metallic target, is projected on a target through a mask to form an illumination pattern on the surface of the photoresist [30]. For this reason, the generated radiation of the 17th harmonic opens possibilities for maskless extreme ultraviolet photolithography, where the illumination pattern on the photoresist is projected point-by-point and the necessary dose for the illumination of the photoresist is acquired in a sinlge-shot regime. This approach makes it possible to refuse the use of a set of technically complex masks, which also absorb a fraction of the energy of radiation used for exposition, which reduces the energy efficiency of a photolithography setup. Furthermore, radiation generation in the gas jet is more favorable compared to generation through the ablation of a metal target due to the absence of the pollution of the optical components by the target ablation products [31].

CONCLUSIONS

To summarize, high (15−25, λ = 83−50 nm) harmonic generation has been realized by 1.24-μm femtosecond radiation of the laser system based on the Cr:forsterite crystal irradiating a dense argon jet under focusing with a relatively high numerical aperture of NA = 0.033. It has been shown that such a focusing requires a high (up to 10 bar) gas jet pressure to improve the geometric phase for optimization of the

Table 1. Parameters of the approximation of the data shown in Fig. 6b

Model	$c + \dfrac{a}{x + b}$	
Plot	Positive chirp	Negative chirp
a	5.83 ± 1.22	61.25 ± 17.43
R^2	0.98	0.99

phase matching and, correspondingly, for maximization of the generation efficiency. It has been demonstrated that the corresponding high density of the gas jet results in a noticeable manifestation of nonlinear propagation effects for generating radiation such as self-phase modulation, self-focusing, and plasma generation with a density of $\sim 10^{17}$ cm^{-3}. All these effects lead to the quasifilament propagation regime of generating radiation near the target and limit its intensity, which in particular result in the saturation of an increase in the optimal pressure with the generating pulse energy and in the spectral broadening of the generated harmonics. It has been established that the compensation of a chirp of the generating pulse, which appears due to self-phase modulation, by the negative prechirping makes it possible to increase the harmonic generation efficiency because of the nonlinear compression of the generating pulse in the process of self-phase modulation. This approach has allowed us to generate the 17th (73 nm) harmonic with an energy of 2 pJ in a pulse at a generation efficiency of 5.4×10^{-9}. Estimates have shown that this radiation can be used for single-pulse maskless photolithography in the extreme ultraviolet range.

CONFLICT OF INTEREST

The authors declare that they have no conflicts of interest.

OPEN ACCESS

REFERENCES

1. E. Appi, C. C. Papadopoulou, J. L. Mapa, et al., Sci. Rep. **10**, 6867 (2020).

2. J. Pupeikis, P.-A. Chevreuil, N. Bigler, L. Gallmann, C. R. Phillips, and U. Keller, Optica **7**, 168 (2020).

3. M. Y. Ryabikin, M. Y. Emelin, and V. V. Strelkov, Phys. Usp. **66**, 382 (2023).

4. A. Andreev, S. Y. Stremoukhov, and O. Shoutova, Laser Phys. **30**, 105402 (2020).

5. B. Mahieu, S. Stremoukhov, D. Gauthier, C. Spezzani, C. Alves, B. Vodungbo, P. Zeitoun, V. Malka, G. de Ninno, and G. Lambert, Phys. Rev. A **97**, 043857 (2018).

6. B. V. Rumiantsev, A. V. Pushkin, D. Z. Suleimanova, N. A. Zhidovtsev, and F. V. Potemkin, JETP Lett. **117**, 566 (2023).

7. J. Zhang, X.-F. Pan, C.-L. Xia, H. Du, T.-T. Xu, and J. Guo, Laser Phys. Lett. **13**, 075302 (2016).

8. I. Babushkin, A. Demircan, U. Morgner, and A. Savel'ev, Phys. Rev. A **106**, 013115 (2022).

9. S. Li, Y. Tang, L. Ortmann, B. K. Talbert, C. I. Blaga, Y. H. Lai, Z. Wang, Y. Cheng, F. Yang, A. S. Landsman, P. Agostini, L. F. DiMauro, Nat. Commun. **14**, 2603 (2023).

10. C. Heyl, C. Arnold, A. Couairon, and A. L'Huillier, J. Phys. B: At. Mol. Opt. Phys. **50**, 013001 (2016).

11. M. Gaponenko, F. Labaye, V. J. Wittwer, C. Paradis, N. Modsching, L. Merceron, A. Diebold, F. Emaury, I. J. Graumann, C. R. Phillips, C. J. Saraceno, C. Kränkel, U. Keller, and T. Südmeyer, in *Nonlinear Optics* (Opt. Publ. Group, Waikoloa, Hawaii, 2017), p. NTh3A-1.

12. V. V. Strelkov, V. T. Platonenko, A. F. Sterzhantov, and M. Y. Ryabikin, Phys. Usp. **59**, 425 (2016).

13. T. Popmintchev, M.-C. Chen, D. Popmintchev, et al., Science (Washington, DC, U. S.) **336** (6086), 1287 (2012).

14. E. Migal, A. Pushkin, B. Bravy, V. Gordienko, N. Minaev, A. Sirotkin, and F. Potemkin, Opt. Lett. **44**, 2550 (2019).

15. B. V. Rumyantsev, K. E. Mikheev, A. V. Pushkin, E. A. Migal, S. Yu. Stremoukhov, and F. V. Potemkin, JETP Lett. **115**, 390 (2022).

16. B. V. Rumyantsev, A. V. Pushkin, K. E. Mikheev, and F. V. Potemkin, Pis'ma Zh. Eksp. Teor. Fiz. **116**, 659 (2022).

17. E. Migal, S. Y. Stremoukhov, and F. Potemkin, Phys. Rev. A **101**, 021401 (2020).

18. E. Migal, F. Potemkin, and V. Gordienko, Laser Phys. Lett. **16**, 045401 (2019).

19. C. Jin, A.-T. Le, and C. Lin, Phys. Rev. A **83**, 023411 (2011).

20. P.-C. Li and S.-I. Chu, Phys. Rev. A **88**, 053415 (2013).

21. V. Cardin, B. Schmidt, N. Thiré, S. Beaulieu, V. Wanie, M. Negro, C. Vozzi, V. Tosa, and F. Légaré, J. Phys. B: At. Mol. Opt. Phys. **51**, 174004 (2018).

22. B. Major, M. Kretschmar, O. Ghafur, A. Hoffmann, K. Kovacs, K. Varjú, B. Senfftleben, J. Tümmler, I. Will, T. Nagy, D. Rupp, M. J. J. Vrakking, V. Tosa, and B. Schütte, J. Phys.: Photon. **2**, 034002 (2020).

23. R. W. Boyd, *Nonlinear Optics* (Academic, New York, 2020).

24. R. Weissenbilder, S. Carlström, L. Rego, C. Guo, C. Heyl, P. Smorenburg, E. Constant, C. Arnold, and A. L'Huillier, Nat. Rev. Phys. **4**, 713 (2022).

25. V. P. Kandidov, S. A. Shlenov, and O. G. Kosareva, Quantum Electron. **39**, 205 (2009).

26. A. Braun, G. Korn, X. Liu, D. Du, J. Squier, and G. Mourou, Opt. Lett. **20**, 73 (1995).

27. J. Rothhardt, M. Krebs, S. Hädrich, S. Demmler, J. Limpert, and A. Tünnermann, New J. Phys. **16**, 033022 (2014).

28. R. R. Alfano, Sci. Am. **295** (6), 86 (2006).

29. H. J. Levinson, Jpn. J. Appl. Phys. **61**.SD, SD0803 (2022).

30. C. Wagner, N. Harned, P. Kuerz, M. Lowisch, H. Meiling, D. Ockwell, R. Peeters, K. van Ingen-Schenau, E. van Setten, J. Stoeldraijer, and B. Thuering, in *Extreme Ultraviolet (EUV) Lithography,* Proc. SPIE **7636**, 512 (2010).

31. M. van de Kerkhof, T. van Empel, M. Lercel, C. Smeets, F. van de Wetering, A. Nikipelov, C. Cloin, A. Yakunin, and V. Banine, in *Extreme Ultraviolet (EUV) Lithography X,* Proc. SPIE **10957**, 191 (2019).

Translated by R. Tyapaev